



**QUEEN'S
UNIVERSITY
BELFAST**

Photon collisions with atoms and ions within an intermediate-energy R-matrix framework

Scott, M. P., Kinnen, A. J., & McIntyre, M. W. (2012). Photon collisions with atoms and ions within an intermediate-energy R-matrix framework. *Physical Review A*, 86(3), 1-8. [032707].
<https://doi.org/10.1103/PhysRevA.86.032707>

Published in:
Physical Review A

Document Version:
Early version, also known as pre-print

Queen's University Belfast - Research Portal:
[Link to publication record in Queen's University Belfast Research Portal](#)

Publisher rights
CC-BY <https://creativecommons.org/licenses/by/3.0/>

General rights
Copyright for the publications made accessible via the Queen's University Belfast Research Portal is retained by the author(s) and / or other copyright owners and it is a condition of accessing these publications that users recognise and abide by the legal requirements associated with these rights.

Take down policy
The Research Portal is Queen's institutional repository that provides access to Queen's research output. Every effort has been made to ensure that content in the Research Portal does not infringe any person's rights, or applicable UK laws. If you discover content in the Research Portal that you believe breaches copyright or violates any law, please contact openaccess@qub.ac.uk.

Photon collisions with atoms and ions within an intermediate-energy R -matrix framework

M. P. Scott,* A. J. Kinnen, and M. W. McIntyre

School of Mathematics and Physics,

Queen's University Belfast, Belfast, BT7 1NN, UK

Abstract

Recent experimental advances in light technology necessitate the availability of sophisticated theoretical models which can incorporate an accurate treatment of double-electron continua. We describe here a new intermediate-energy R -matrix approach to photoionisation and photo-double-ionisation and illustrate its feasibility by application to photoionisation and photo-double-ionisation of He, and photodetachment and photo-double-detachment of H^- . Results are shown to be in excellent agreement with previous theoretical and experimental studies. This work is a key step in the development of a multipurpose R -matrix code for multiple-electron ejection.

PACS numbers: 03.65 Nk

*m.p.scott@qub.ac.uk

I. INTRODUCTION

Recent advances in the field of attosecond science (see *e.g.* Corkum and Krausz [1]) yield an enhanced insight into time-resolved dynamics of ultrafast laser-driven excitations of atoms and ions. In addition, the advancement of X-ray free-electron laser sources, such as the Linac Coherent Light Source (LCLS) at the SLAC National Accelerator Laboratory, is generating exciting new experimental data for inner-shell photoionisation processes (see *e.g.* Rohinger *et al.* [2]). In both areas, the light fields contain highly energetic photons with sufficient energy that absorption can lead to the excitation and/or emission of several electrons. A full interpretation of experimental results thus necessitates an understanding of multi-electron dynamics, and two-electron dynamics in particular.

To complement the experimental advances in light technology, it is essential to have advanced theoretical models which incorporate an accurate treatment of double-electron continua, both within a time-dependent and time-independent framework. While the time-independent R -matrix method for photoionisation has been in worldwide use for many years (see *e.g.* Burke and Taylor [3]), it is only recently that an *ab initio* time-dependent R -matrix approach has been developed to facilitate the study of the interaction of ultrashort light fields with many-electron atoms and ions (Lysaght *et al.* [4], Moore *et al.* [5]). We now seek a suitable R -matrix based approach to incorporate double-electron continua. Towards this end, we report here the development and implementation of a new intermediate-energy R -matrix (IERM) approach to photoionisation and photo-double-ionisation, and investigate the suitability of this method by comparing results for photoionisation and photo-double-ionisation of He, and photodetachment and photo-double-detachment of H^- , with existing theoretical and experimental data.

The IERM approach for the accurate description of double-electron continua has already proved highly successful in the study of electron collisions with one-electron systems [6–8]. This current work focuses on photon collisions with two-electron systems within a time-independent framework. This is an essential first step towards our ultimate goal of the development of many-electron, time-dependent and time-independent R -matrix codes, capable of accurate treatment of double-electron continua. Such codes will also be able to provide accurate data to assess the feasibility of planned experimental studies at leading-edge facilities.

The rest of this paper is organised as follows: in Sec. II we derive the IERM theory for photon collisions with two-electron atoms and ions, while in Sec. III and Sec. IV we present results for photoionisation and photo-double-ionisation of He and photodetachment and photo-double-detachment of H^- . Conclusions are drawn in Sec. V.

II. THEORY

The differential cross section for photoionisation of a two-electron atom or ion with the ejection of the photoelectron in the direction $\hat{\mathbf{k}}$ is given, in the length approximation, by

$$\frac{d\sigma_L}{d\hat{\mathbf{k}}} = 8\pi^2 \alpha a_0^2 \omega |\langle \Psi_f^-(\hat{\mathbf{k}}) | \hat{\mathbf{e}} \cdot \mathbf{M} | \Psi_i \rangle|^2, \quad (1)$$

where

$$\mathbf{M} = \mathbf{r}_1 + \mathbf{r}_2. \quad (2)$$

α is the fine structure constant, a_0 is the Bohr radius of the hydrogen atom and ω is the incident photon energy in a.u., while $\hat{\mathbf{e}}$ is the polarisation vector. The initial and final state wavefunctions, Ψ_i and $\Psi_f^-(\hat{\mathbf{k}})$, are solutions of the Schrodinger equation

$$(H - E)\Psi = 0, \quad (3)$$

where H is the two-electron Hamiltonian operator,

$$H = \left(-\frac{1}{2} \nabla_1^2 - \frac{Z}{r_1} \right) + \left(-\frac{1}{2} \nabla_2^2 - \frac{Z}{r_2} \right) + \frac{1}{r_{12}}. \quad (4)$$

The initial state, Ψ_i , has total orbital angular momentum L_i , total spin angular momentum, S_i and parity Π_i ; the final two-electron state, consisting of the residual ion plus photoelectron, has corresponding quantum numbers L , S and Π , respectively. The orbital angular momentum, spin angular momentum and parity of the residual one-electron ion are L_f , S_f and Π_f . The final state wavefunction, $\Psi_f^-(\hat{\mathbf{k}})$, satisfies the boundary condition corresponding to a plane wave in the direction $\hat{\mathbf{k}}$ incident on the residual ion, with ingoing waves in all open channels. Ψ_i and $\Psi_f^-(\hat{\mathbf{k}})$ are normalised so that

$$\langle \Psi_i | \Psi_i \rangle = 1 \quad (5)$$

and

$$\langle \Psi_f^-(\hat{\mathbf{k}}) | \Psi_{f'}^-(\hat{\mathbf{k}}') \rangle = \delta_{ff'} \delta\left(\frac{1}{2}k^2 - \frac{1}{2}k'^2\right) . \quad (6)$$

The total cross section for photoionisation by unpolarized light can be obtained by integrating Eq.(1) over all photoelectron angles, $\hat{\mathbf{k}}$, and averaging over all photon polarisation directions. This gives the following expression for the total cross section:

$$\sigma = \frac{8\pi^2 \alpha a_0^2 \omega}{3(2L_i + 1)} \sum_{\ell_f L} |\langle \Psi_f^- \| M \| \Psi_i \rangle|^2 . \quad (7)$$

The summation in (7) is over all possible final state orbital angular momenta, L , of the two-electron system permitted by dipole selection rules, and over permitted orbital angular momenta, ℓ_f , of the ejected photoelectron. We have introduced the reduced dipole matrix element in the summation on the right-hand-side of (7) which, according to the Wigner-Eckart theorem, is given by

$$\langle \Psi_f^- \| M \| \Psi_i \rangle = \frac{(2L + 1)^{\frac{1}{2}}}{C(L_i 1 L_f; M_{L_i} \mu M_{L_f})} \langle \Psi_f^- | M^\mu | \Psi_i \rangle . \quad (8)$$

As in the application of R -matrix theory to other atomic collision processes, configuration space is divided into two regions using a sphere of radius $r = a$, centred on the target nucleus; r , in this application, being the relative radial coordinate of the photoelectron. In the internal region, both Ψ_i and Ψ_f^- are expanded in terms of appropriate sets of energy-independent, two-electron R -matrix basis functions $\{\Theta_k^{L_i S_i \Pi_i}(\mathbf{r}_1, \mathbf{r}_2)\}$ and $\{\Theta_k^{L S \Pi}(\mathbf{r}_1, \mathbf{r}_2)\}$ as follows:

$$\Psi_i = \sum_k A_{ki} \Theta_k^{L_i S_i \Pi_i} \quad (9)$$

$$\Psi_f^- = \sum_k A_{kf} \Theta_k^{L S \Pi} . \quad (10)$$

The R -matrix basis sets $\{\Theta_k^{L_i S_i \Pi_i}(\mathbf{r}_1, \mathbf{r}_2)\}$ and $\{\Theta_k^{L S \Pi}(\mathbf{r}_1, \mathbf{r}_2)\}$ are constructed from two-electron functions $\chi_{n_1 \ell_1 n_2 \ell_2}(\mathbf{r}_1, \mathbf{r}_2)$:

$$\Theta_k^{L_i S_i \Pi_i} = \sum_{n'_1 \ell'_1 n'_2 \ell'_2} \chi_{n'_1 \ell'_1 n'_2 \ell'_2}^{L_i S_i \Pi_i}(\mathbf{r}_1, \mathbf{r}_2) \beta_{n'_1 \ell'_1 n'_2 \ell'_2 k}^{L_i S_i \Pi_i} \quad (11)$$

and

$$\Theta_k^{LS\Pi} = \sum_{n_1 \ell_1 n_2 \ell_2} \chi_{n_1 \ell_1 n_2 \ell_2}^{LS\Pi}(\mathbf{r}_1, \mathbf{r}_2) \beta_{n_1 \ell_1 n_2 \ell_2 k}^{LS\Pi} . \quad (12)$$

We note that

$$\begin{aligned} \chi_{n_1 \ell_1 n_2 \ell_2}^{LS\Pi}(\mathbf{r}_1, \mathbf{r}_2) &= \frac{1}{\sqrt{2}} \{ r_1^{-1} r_2^{-1} u_{n_1 \ell_1}(r_1) u_{n_2 \ell_2}(r_2) \mathcal{Y}_{\ell_1 \ell_2 LM_L}(\hat{\mathbf{r}}_1, \hat{\mathbf{r}}_2) \\ &+ (-)^{\ell_1 + \ell_2 + L + S} r_1^{-1} r_2^{-1} u_{n_1 \ell_1}(r_2) u_{n_2 \ell_2}(r_1) \mathcal{Y}_{\ell_2 \ell_1 LM_L}(\hat{\mathbf{r}}_1, \hat{\mathbf{r}}_2) \} \text{ if } n_1 \ell_1 \neq n_2 \ell_2 \end{aligned}$$

and

$$\chi_{n \ell n \ell}^{LS\Pi}(\mathbf{r}_1, \mathbf{r}_2) = r_1^{-1} r_2^{-1} u_{n \ell}(r_1) u_{n \ell}(r_2) \mathcal{Y}_{\ell \ell LM_L}(\hat{\mathbf{r}}_1, \hat{\mathbf{r}}_1) \text{ if } n_1 \ell_1 = n_2 \ell_2 . \quad (13)$$

In Eq. (13) the radial functions $u_{n \ell}(r)$ are solutions of the second-order differential equation

$$\left(\frac{d^2}{dr^2} - \frac{\ell(\ell+1)}{r^2} + \frac{2Z}{r} + k_{n \ell}^2 \right) u_{n \ell}(r) = 0 , \quad (14)$$

subject to the boundary conditions

$$\begin{aligned} u_{n \ell}(0) &= 0 \\ \left(\frac{a}{u_{n \ell}} \right) \frac{du_{n \ell}}{dr} \Big|_{r=a} &= 0 . \end{aligned}$$

We choose the R -matrix boundary radius, $r = a$, sufficiently large so that the radial functions of the physical states of interest of the residual ion are completely enveloped by this boundary and generated by Eq. (14). We also ensure that the initial state wavefunction, Ψ_i , is completely enclosed within the interaction volume defined by $r = a$. The angular functions, $\mathcal{Y}_{\ell_1 \ell_2 LM_L}(\hat{\mathbf{r}}_1, \hat{\mathbf{r}}_2)$ are defined by

$$\mathcal{Y}_{\ell_1 \ell_2 LM_L}(\hat{\mathbf{r}}_1, \hat{\mathbf{r}}_2) = \sum_{m_{\ell_1}, m_{\ell_2}} C(\ell_1 \ell_2 L; m_{\ell_1} m_{\ell_2} M_L) Y_{\ell_1 m_{\ell_1}}(\hat{\mathbf{r}}_1) Y_{\ell_2 m_{\ell_2}}(\hat{\mathbf{r}}_2) . \quad (15)$$

The coefficients $\beta_{n_1 \ell_1 n_2 \ell_2 k}$ in Eq. (13) are obtained by diagonalising the appropriate two-electron Hamiltonian matrix. This ensures that the R -matrix basis functions $\{\Theta_k^{L_i S_i \Pi_i}(\mathbf{r}_1, \mathbf{r}_2)\}$ and $\{\Theta_k^{LS\Pi}(\mathbf{r}_1, \mathbf{r}_2)\}$ satisfy

$$\langle \Theta_k^{L_i S_i \Pi_i}(\mathbf{r}_1, \mathbf{r}_2) | H | \Theta_{k'}^{L_i S_i \Pi_i}(\mathbf{r}_1, \mathbf{r}_2) \rangle = \delta_{kk'} E_{ki} \quad (16)$$

and

$$\langle \Theta_k^{L\Sigma}(\mathbf{r}_1, \mathbf{r}_2) | H | \Theta_{k'}^{L\Sigma}(\mathbf{r}_1, \mathbf{r}_2) \rangle = \delta_{kk'} E_{kf} , \quad (17)$$

respectively.

Returning to Eq. (9) and Eq. (10), the expansion coefficients A_{ki} and A_{kf} are given by (see *e.g.* Burke and Taylor [3])

$$A_{ki} = \frac{1}{2a(E_{ki} - E_i)} \sum_j w_{jk}(a) \left(a \frac{dy_{ji}}{dr} - by_{ji} \right)_{r=a} \quad (18)$$

and

$$A_{kf} = \frac{1}{2a(E_{kf} - E_i - \omega)} \sum_j w_{jk}(a) \left(a \frac{dy_{jf}^-}{dr} - by_{jf}^- \right)_{r=a} , \quad (19)$$

where E_i is the energy of the initial state. $w_{jk}(a)$ are surface amplitudes, defined in terms of the radial functions, $u_{n_1 l_1}(a)$, on the boundary of the internal region by

$$\omega_{jk}(a) = \sum_{n_1} \beta_{n_1 \ell_1 n_2 \ell_2} u_{n_1 \ell_1}(a) , j \equiv n_2 \ell_2 \ell_1 . \quad (20)$$

We note that the surface amplitudes $\omega_{jk}(a)$ in (18) and (19) are not the same, since Ψ_i and Ψ_f^- have different angular symmetries and a different set of surface amplitudes will be obtained for the initial and final state calculations. y_{ji} and y_{jf}^- describe the radial motion of the photoelectron in channel j in the initial and final states respectively. These functions satisfy the equation

$$y_{jp}(a) = \sum_{t=1}^{nchan} R_{jt} \left(\frac{dy_{tp}}{dr} - by_{tp} \right)_{r=a} \quad j = 1, \dots, nchan , \quad (21)$$

where p represents either i or f as appropriate, and R_{jt} are elements of the multi-channel \mathbf{R} -matrix. $nchan$ is the total number of channels. Rewriting (21) in matrix notation we obtain

$$\mathbf{y}(a) = \mathbf{R} \times \left(a \frac{d\mathbf{y}_p}{dr} - b\mathbf{y}_p \right)_{r=a} . \quad (22)$$

Substituting Eq. (22) into Eq. (18) and Eq. (19) yields the expressions

$$A_{ki} = \mathbf{G}_i \mathbf{W}_{ki}^T(a) \mathbf{R}_i^{-1} \mathbf{y}_i(a) \quad (23)$$

$$A_{kf} = \mathbf{G}_f \mathbf{W}_{kf}^T(a) \mathbf{R}_f^{-1} \mathbf{y}_f(a) , \quad (24)$$

where we have introduced the diagonal matrices \mathbf{G}_i and \mathbf{G}_f :

$$\mathbf{G}_i = \frac{1}{2a(E_{ki} - E_i)} \quad \text{and} \quad (25)$$

$$\mathbf{G}_f = \frac{1}{2a(E_{kf} - E_i - \omega)} \quad . \quad (26)$$

We define matrices \mathbf{V}_i and \mathbf{V}_f , whose columns consist of the β coefficients introduced in (13), i.e.

$$V_{i_{t'k}} = \beta_{t'k}^{L_i S_i \Pi_i} \quad , \quad t' \equiv n'_1 \ell'_1 n'_2 \ell'_2 \quad (27)$$

and

$$V_{f_{tk}} = \beta_{tk}^{LS\Pi} \quad , \quad t \equiv n_1 \ell_1 n_2 \ell_2 \quad . \quad (28)$$

Defining the reduced dipole matrix, \mathbf{M} , by

$$\mathbf{M} = \langle \chi_{n_1 \ell_1 n_2 \ell_2}^{LS\Pi} \| M \| \chi_{n'_1 \ell'_1 n'_2 \ell'_2}^{L_i S_i \Pi_i} \rangle \quad , \quad (29)$$

it is possible to rewrite the expression for the photoionisation cross section, σ , as

$$\sigma = \frac{8\pi^2 \alpha a_0^2 \omega}{3(2L_i + 1)} \sum_{\ell_f L} |\mathbf{y}_f^T \mathbf{R}_f^{-1} \mathbf{W}_f \mathbf{G}_f \mathbf{V}_f^T \mathbf{M} \mathbf{V}_i \mathbf{G}_i \mathbf{W}_i^T \mathbf{R}_i^{-1} \mathbf{y}_i|^2 \quad . \quad (30)$$

We will assume that the interaction volume is sufficiently large and our approximation sufficiently accurate so that the energy of the initial state, E_i , is extremely close to one of the eigenvalues, $E_{k'i}$, in Eq. (23), and that the contribution to the initial state wavefunction from closed channels in the external region, as represented by Eq. (21), can be neglected. The expression for A_{ki} then simplifies considerably to:

$$A_{ki} = \begin{cases} 1 & \text{if } k = k' \\ 0 & \text{otherwise} \end{cases} \quad (31)$$

(30) then reduces to

$$\sigma = \frac{8\pi^2 \alpha a_0^2 \omega}{3(2L_i + 1)} \sum_{\ell_f L} |\mathbf{y}_f^T \mathbf{R}_f^{-1} \mathbf{W}_f \mathbf{G}_f \mathbf{V}_f^T \mathbf{M} \mathbf{V}_{i_{k'}}|^2 \quad , \quad (32)$$

where $\mathbf{V}_{i_{k'}}$ is the eigenvector of the initial state Hamiltonian matrix associated with the eigenvalue $E_{k'i}$. Provided that $E_{k'i}$ is sufficiently close to the experimental value for E_i , it is possible to improve our theoretical value for the initial state energy by making a very

small adjustment to the appropriate diagonal element of the Hamiltonian matrix, prior to diagonalisation.

All entities in Eq. (32) are evaluated within the internal region except for \mathbf{y}_f^T , which is obtained by solving the scattering problem for the residual ion in the external region, and matching to the inner region solution on the boundary through the R -matrix, as illustrated by Eq. (22). One of the advantages of the R -matrix method is that the bulk of the computational work lies in the construction and diagonalisation of the Hamiltonian matrix in the internal region which, being energy-independent, needs to be carried out only once for each partial wave. The energy-dependence appears in the denominator of the R -matrix and in the evaluation of \mathbf{y}_f^T in the external region, which are considerably less onerous. As such, it is relatively easy to calculate cross sections over a very fine energy mesh, once the inner region problem has been solved.

To test the above theory we have applied the IERM method for photoionisation to photoionisation and photo-double-ionisation of He and photodetachment and photo-double-detachment of H^- . Details of these calculations are given in the next section.

III. PHOTOIONISATION AND PHOTO-DOUBLE-IONISATION OF HE

A. Calculation

We first consider photoionisation of the $1S^e$ ground state of He with the emission of a single electron, focusing on the energy region between the $n = 2$ and $n = 3$ thresholds, due to the wealth of existing data with which to compare. In our study a boundary radius of 40.0 a.u. was employed, which completely enveloped the He ground state and the He^+ states of interest. As seen from Sec. II, the two-electron wavefunction for the ground state of He is described in terms of products of one-electron He^+ orbitals. Clearly, the He^+ $1s$ orbital and the He $1s$ orbital of the $1s^2 1S^e$ ground state are significantly different. Hence, if we are to use the He^+ one-electron orbital basis, it is essential that this basis contains a sufficiently large number of pseudo-orbitals to correct for this. We have therefore used a one-electron orbital basis for the He^+ residual ion consisting of the physical orbitals $1s, 2s, 2p, 3s, 3p, 3d, 4s, 4p, 4d$ and $4f$, augmented by pseudo-orbitals $n = 5$ to $n = 38$, with angular momentum $\ell = 0, \dots, 4$. As well as improving the initial He ground state, the additional pseudo-orbitals give rise to

non-physical pseudo-states, whose inclusion provides a mechanism for the study of photo-double-ionisation. The radial functions for all orbitals have been generated using Eq. (14) and, provided the boundary radius is sufficiently large, the required physical He^+ orbitals are obtained. The ‘bound’ photoelectron in the initial state and the ejected photoelectron in the $^1P^o$ final state are described in terms of the same one-electron basis, except that a total of 80 radial functions (or ‘continuum functions’) were included per angular momentum, ℓ , where, in the final state, $\ell = 0, \dots, 5$. This meant that the same approximation was used in the construction of the R -matrix basis functions in both the initial and final states. The ground state energy was calculated as -2.8997 a.u.. However, by making a small adjustment of -0.0042 a.u. to the diagonal element dominating the calculation of the associated eigenvalue before diagonalisation, it was possible to bring the ground state energy into agreement with the non-relativistic limit of -2.9037 a.u. reported by Perekis [10].

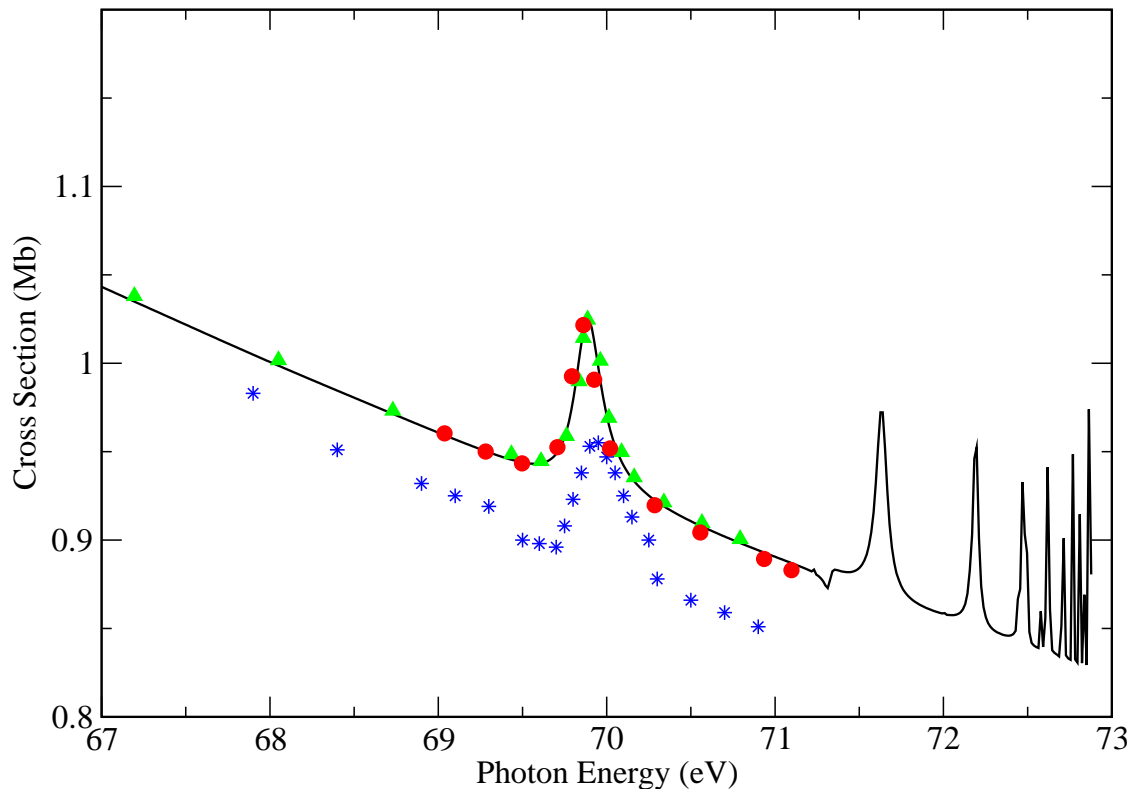


FIG. 1: (Color online) Partial cross section for photoionisation of the $1s^e$ ground state of He to the $1s$ state of He^+ . (Solid line) Present results. (Triangles) Xu and Shakeshaft [9]. (Circles) Jiang *et al.* [11]. (Stars) Lindle *et al.* [12].

To estimate the photo-double-ionisation cross section we sum the cross section to the

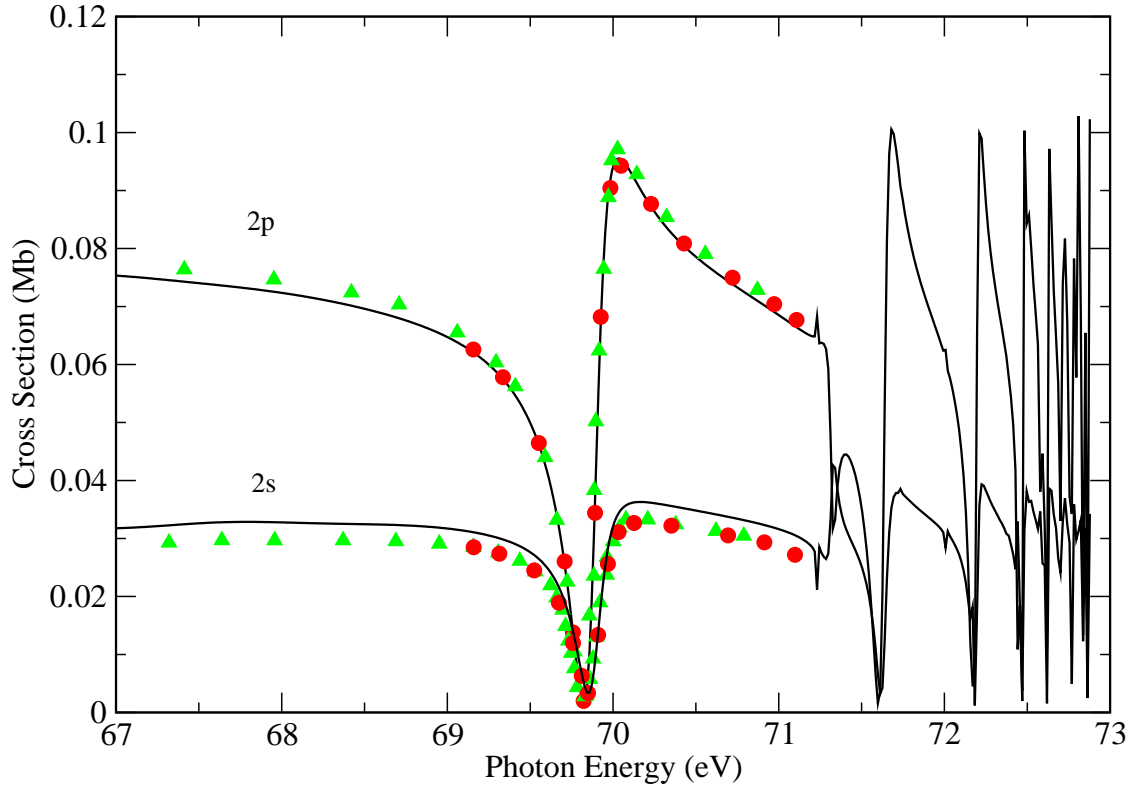


FIG. 2: (Color online) Partial cross section for photoionisation of the $1S^e$ ground state of He to the $2s$ and $2p$ states of He^+ . (Solid line) Present results. (Triangles) Xu and Shakeshaft [9]. (Circles) Jiang *et al.* [11].

positive-energy pseudo-states lying above the double-ionisation threshold. A correction has been incorporated to account for the contribution from negative-energy pseudo-states lying close to threshold, and to eliminate any over-estimate from positive-energy pseudo-states immediately above threshold. In evaluating the photo-double-ionisation cross section we have carried out two calculations. In the energy region from the double-ionisation threshold to about 10 eV above this threshold we have extended the R -matrix boundary radius to 70 a.u. in order to increase the density of pseudo-states. We have increased the residual ion basis to include an additional 38 pseudo-states per angular momentum, giving a total of 162 He^+ target states, of which 126 lie above the double-ionisation threshold. At higher energies we have used an R -matrix boundary of 40.0 a.u., which, although giving a less dense pseudo-state basis, spans a much greater energy range. Throughout our calculations we have carefully checked convergence with respect to the R -matrix boundary radius, the number and density of pseudo-states and the number of radial continuum functions.

B. Results

In Fig. 1 and Fig. 2 we present results for photoionisation cross sections to the $1s, 2s$ and $2p$ states of He^+ , for photon energies in the region 67.0 - 72.5 eV. The dominant feature in this energy region is the series of resonances converging onto the $\text{He}^+ n = 3$ threshold. In particular, we concentrate on the closed-channel resonance around 70 eV, and compare our results with the recent work of Xu and Shakeshaft [9], and with previous R -matrix calculations of Jiang *et al.* [11]. Our results are generally in good agreement with both these studies, although our data for the $2s$ cross section lie slightly higher. In Fig. 1 we have also included the experimental results of Lindle *et al.* [12], which tend to lie about 5 % lower than theory. For clarity we have not included the results reported by Jiang *et al.* above 71 eV, but similar agreement is obtained at higher energies.

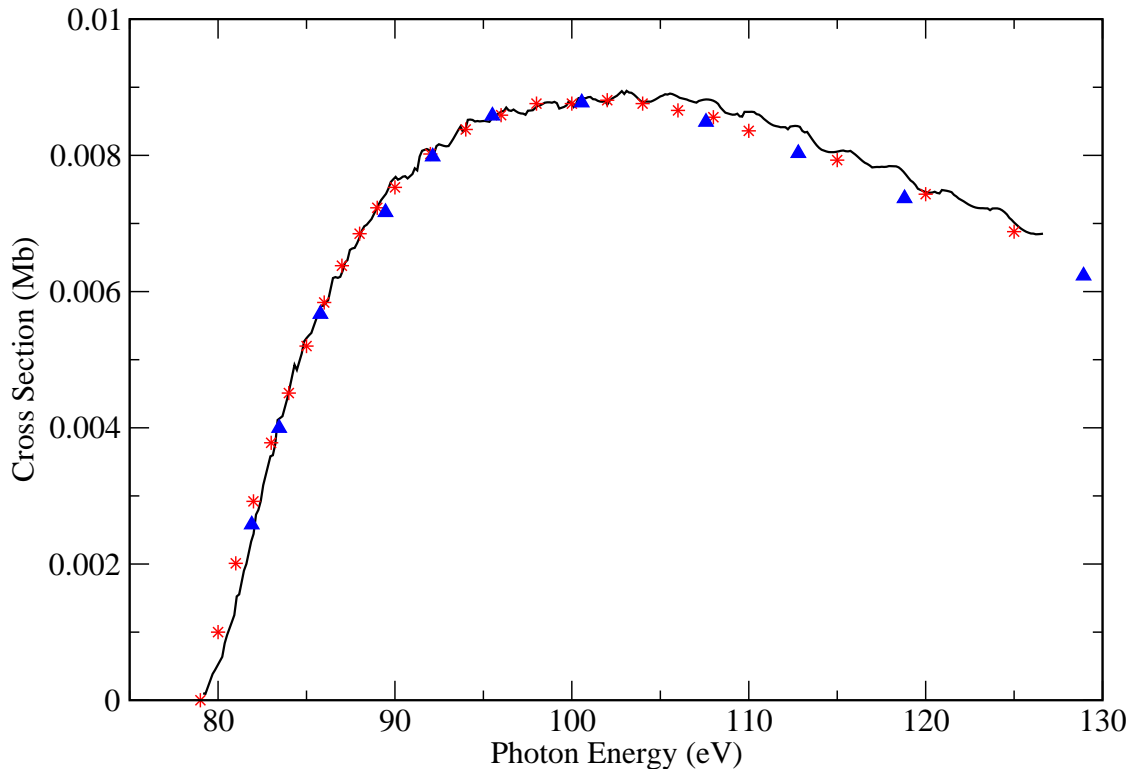


FIG. 3: (Color online) Photo-double-ionisation cross section of He. (Solid line) Present results (unsmoothed). (Stars) Samson *et al.* [15]. (Triangles) Ludlow *et al.* [16].

In Fig. 3 and Fig. 4 we give results for the photo-double-ionisation calculation by considering the absolute photo-double-ionisation cross section and the percentage ratio of double-ionisation to single-ionisation in the photon energy range 79 - 130 eV. The results

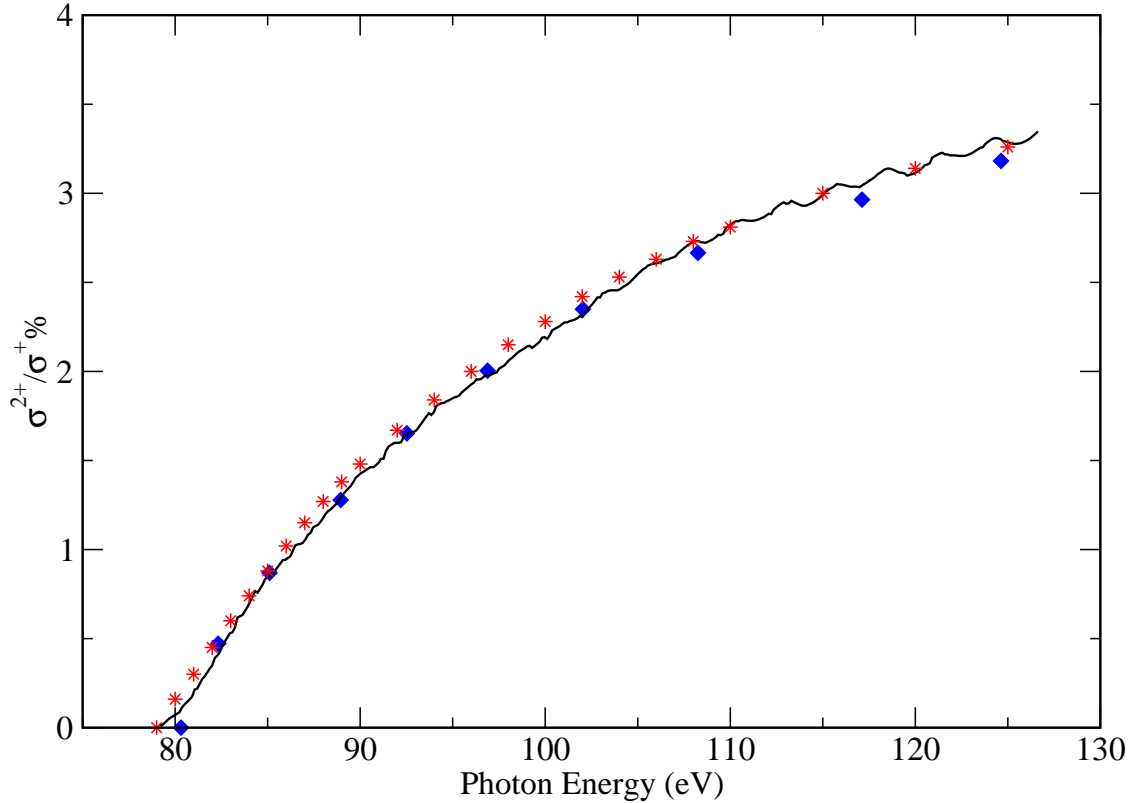


FIG. 4: (Color online) Percentage ratio of double-ionisation to single-ionisation in the photoionisation of He. (Solid line) Present results (unsmoothed). (Stars) Samson *et al.* [15]. (Diamonds) Kheifets and Bray [17].

that are presented exhibit small oscillations which is due to the onset of numerous pseudo-state thresholds. These oscillations diminish with increasing pseudo-state density and can be removed by a number of techniques including ‘T-matrix averaging’ (see *e.g.* Burke *et al.* [13]) and ‘box averaging’ (see *e.g.* Bartschat and Bray [14]). Alternatively, when the oscillations are very small, smoothing of the cross section using a Chebyshev-series least squares procedure will suffice. We compare our results with the experimental data of Samson *et al.* [15] and with the time-dependent close-coupling calculations of Ludlow *et al.* [16] and the convergent close coupling (CCC) data of Kheifets and Bray [17]. Our evaluations are seen to be in excellent agreement with theory and experiment for both observables.

IV. PHOTODETACHMENT AND PHOTO-DOUBLE-DETACHMENT OF H^-

A. Calculation

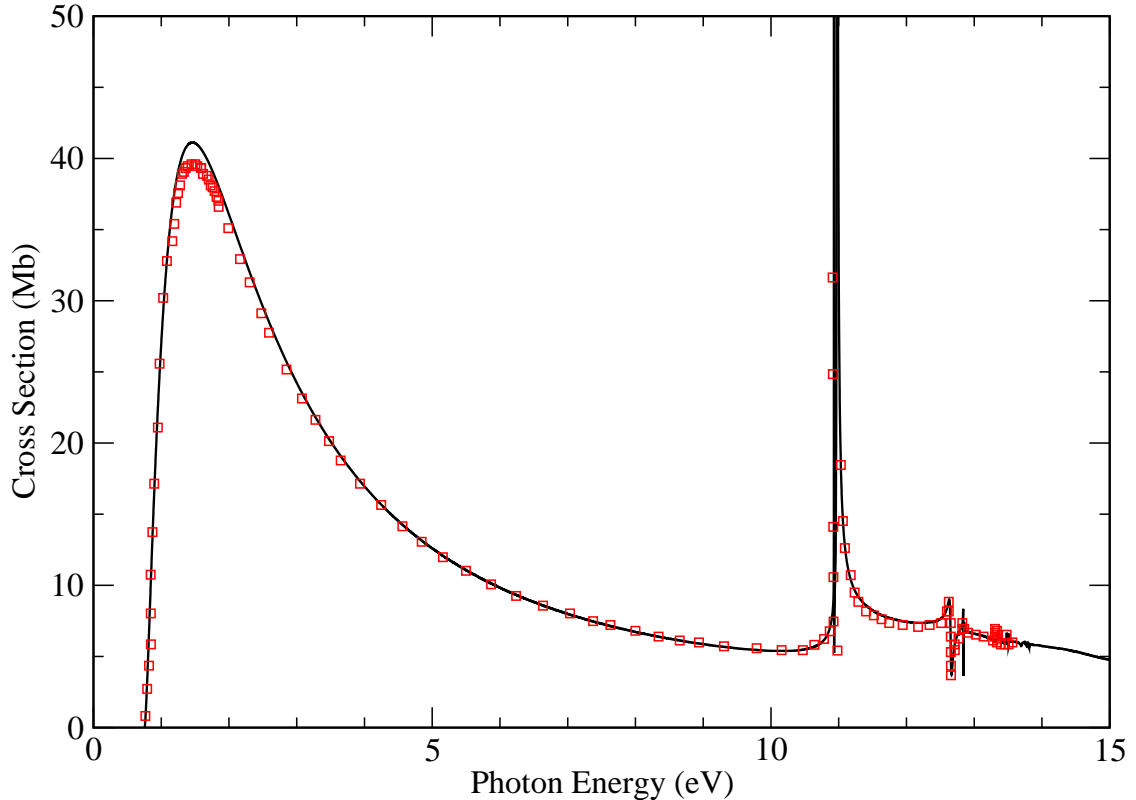


FIG. 5: (Color online) Total photodetachment cross section of H^- up to the $n = 5$ threshold of H. (Solid line) Present results. (Squares) Miyake *et al.* [20].

We first consider photodetachment of the $1S^e$ ground state of H^- , leaving the H atom in the state $n\ell$, where $n \leq 5$ and $\ell \leq 4$, as permitted. Due to the degeneracy of the atomic H energy levels for a particular n , $E_{n\ell}$, ($\ell = 0, \dots, n-1$), angular momentum exchange effects exist between the H^- electrons, even out to extremely large distances. For this reason, we have extended the R -matrix radius to 350 a.u., to accurately describe some of the resonance features present in the low energy region. 200 continuum functions were required to obtain converged results. The ground state energy of H^- was calculated as -0.523136 a.u., but this was brought into agreement with the highly accurate non-relativistic energy of -0.527751 a.u., calculated by Drake [18], by making an adjustment of -0.00812 a.u. to the appropriate diagonal element of the two-electron Hamiltonian matrix

prior to diagonalisation, as described earlier.

B. Results

In Fig. 5 we give an overview of our results for the total cross section for photodetachment of H^- in the photon energy range 0 - 14 eV, i.e. to just above the H $n = 5$ threshold. Our results are compared with the recent results reported by Miyake *et al.* [20], where a hybrid approach has been adopted which combines R -matrix calculations with high-resolution cross section measurements and previous theoretical results. We note that our *ab initio* data are generally in good agreement with these data throughout the energy region considered, except for the height of the peak at around 2 eV, where the current results lie slightly lower.

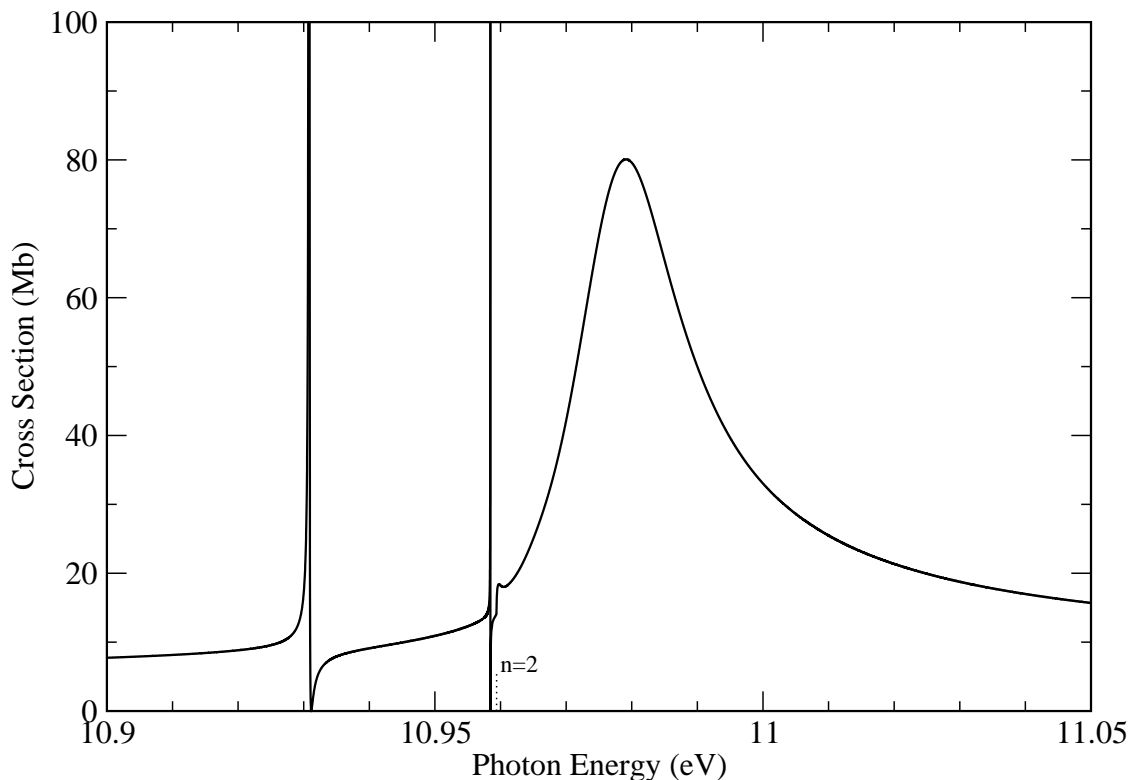


FIG. 6: Total photodetachment cross section of H^- near the $n = 2$ threshold of H .

In Fig. 6 and Fig. 7 we show the total photodetachment cross section in the energy region around the $n = 2$ and $n = 3$ thresholds of H . These energy regions are dominated by shape and closed-channel Feshbach resonances: detailed results for the width, Γ , and position, E_r , of these structures are given in Table I and Table II. Γ , and E_r have been obtained by fitting

the eigenphase sum, δ_S , to the form

$$\delta_S = \delta_0 + \delta_1 E + \delta_2 E^2 + \arctan\left(\frac{\Gamma}{E_r - E}\right) \quad (33)$$

where E is the energy of the photoelectron. In Tables I and II we give the resonance position in terms of the total energy, E_{tot} of the residual H atom in a.u., while the width, Γ , is presented in eV.

TABLE I: Theoretical comparison of widths and positions of resonances in the photodetachment cross section of H^- near the $n = 2$ threshold of H.

Source	$E_{tot}(\text{a.u.})$	$\Gamma(\text{eV})$
Present	-0.12605	0.0000389
Lindroth ^a	-0.12605	0.000034
Sadeghpour <i>et al.</i> ^b	-0.126014	0.0000288
Tang <i>et al.</i> ^c	-0.12606	0.000065
Ho ^d	-0.1260498	0.0000359
Present	-0.12503	0.00000024
Lindroth	-0.12504	<0.0000002
Tang <i>et al.</i>	-0.12503	
Present	-0.12450	0.0167
Lindroth	-0.12437	0.0185
Sadeghpour <i>et al.</i>	-0.124242	0.0186
Tang <i>et al.</i>	-0.12432	0.0169
Ho and Bhatia ^e	$-0.12436 \pm 3 \times 10^{-5}$	$0.0188 \pm 2 \times 10^{-4}$

^aRef. [19] ^bRef. [21] ^cRef. [22] ^dRef. [23] ^eRef. [24]

We compare our results with those of Lindroth [19], Sadeghpour *et al.* [21], Tang *et al.* [22] and Ho [23] and Ho and Bhatia [24]. Lindroth carried out an extremely accurate and detailed study of the photodetachment of H^- , using a complex rotation approach in combination with a discrete numerical basis to form highly correlated descriptions of both the initial and final states. Sadeghpour *et al.* have performed an extensive eigenchannel R -matrix calculation, while the data of Tang *et al.* has been obtained using a hyperspherical

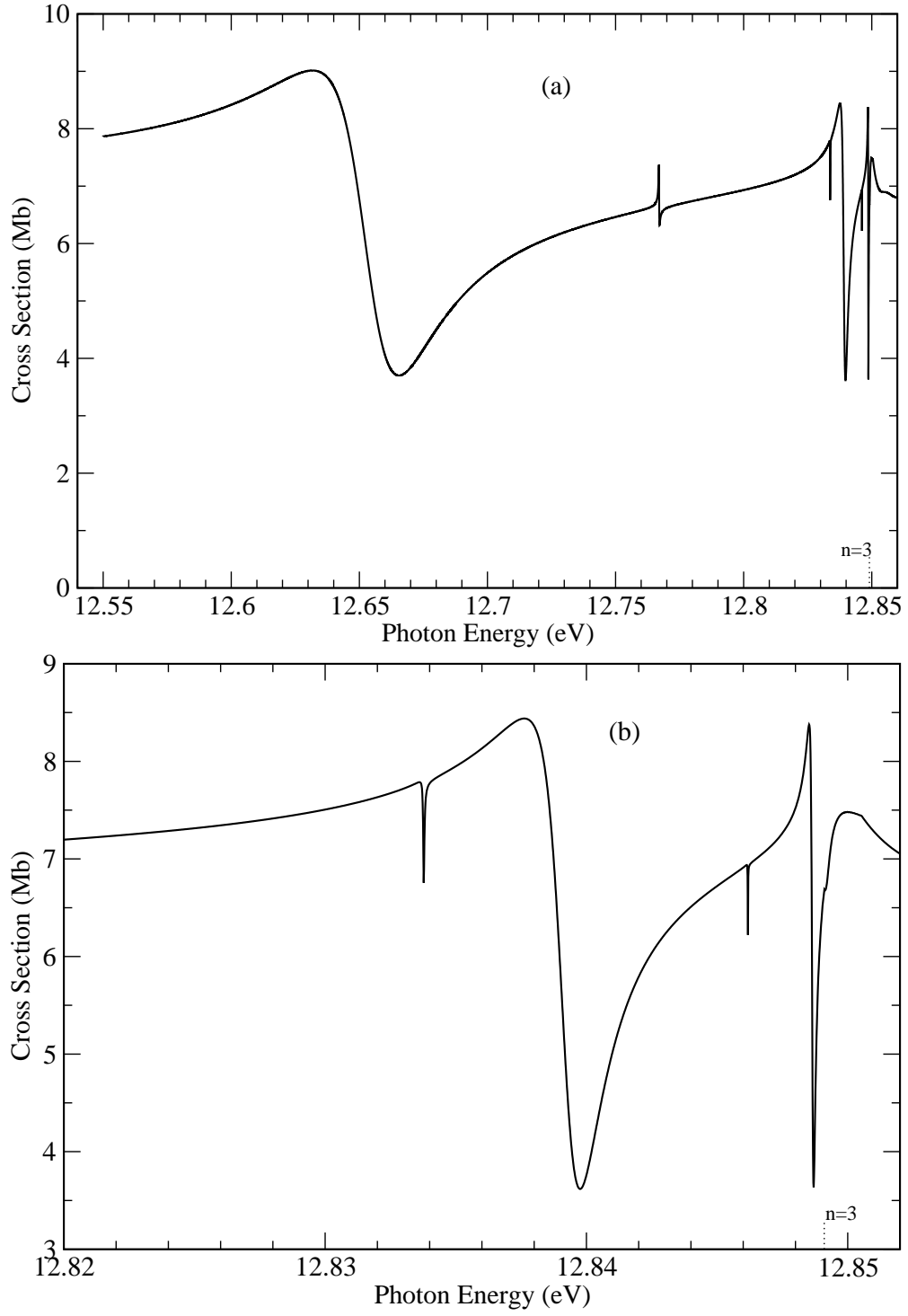


FIG. 7: Total photodetachment cross section of H^- near the $n = 3$ threshold of H . The region close to threshold is shown in more detail in (b)

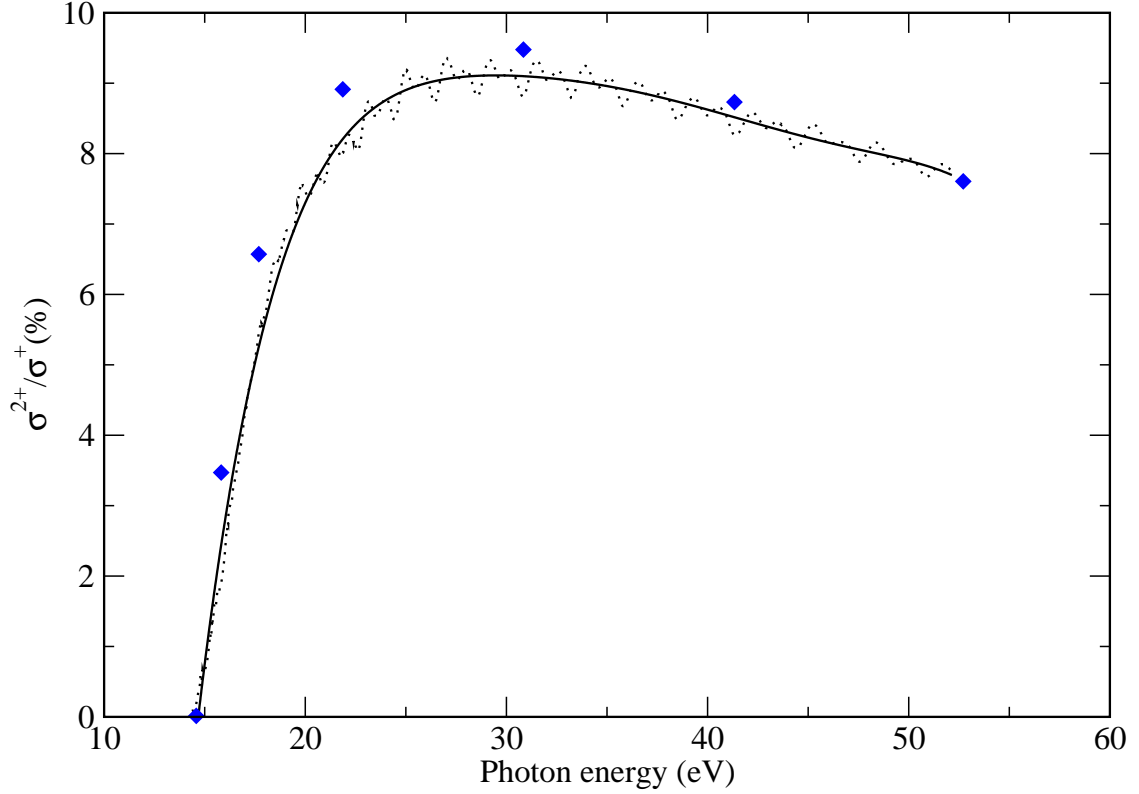


FIG. 8: (Color online) Percentage ratio of double-ionisation to single-ionisation in the photodetachment cross section of H^- . (Solid line) Present results (smoothed). (Dotted line) Present results (unsmoothed). (Diamonds) Kheifets and Bray [17]

close-coupling approach. The work of Ho and Ho and Bhatia employed Hylleraas wave functions with the use of complex rotation. Hylleraas wavefunctions afford a very accurate treatment of correlation effects.

In Fig. 6 we observe three distinct resonances. The first resonance is associated with a doubly excited state dominated by the configurations $2snp$ and $2pns$, while the second extremely narrow resonance is due to a Rydberg-type state. The broad shape resonance just above the $n = 2$ threshold is dominated by configurations of the form $2snp$, $2pns$ and $2pnd$, and has been the subject of detailed study by various theoretical methods. In particular the height of the peak was investigated by Tang *et al.*, who concluded that this value was related to the accuracy of the initial-state wavefunction for H^- . They reported a value of 78.6 Mb for the approximation which they considered to be most accurate. The height of this peak from the current work is 80.09 Mb, while Lindroth reports a value of 76 Mb. We see from Table I that our results are in excellent agreement with the other theoretical results

TABLE II: Theoretical comparison of widths and positions of resonances in the photodetachment cross section of H^- near the $n = 3$ threshold of H.

Source	$E_{tot}(\text{a.u.})$	$\Gamma(\text{eV})$
Present	-0.06271	0.0322
Lindroth ^a	-0.06273	0.0326
Sadeghpour <i>et al.</i> ^b	-0.062695	0.0334
Tang <i>et al.</i> ^c	-0.06272	0.0326
Ho ^d	-0.06271675	0.03240
Present	-0.05857	0.00024
Lindroth	-0.05857	0.00024
Sadeghpour	-0.058866	0.000402
Tang <i>et al.</i>	-0.05859	0.000261
Ho	-0.0585718	0.0002444
Present	-0.05612	0.000054
Lindroth	-0.05612	0.00006
Tang <i>et al.</i>	-0.05614	
Ho	-0.0561167	0.000057
Present	-0.05592	0.00183
Lindroth	-0.05590	0.00193
Sadeghpour	-0.055832	0.00116
Tang <i>et al.</i>	-0.05591	0.00155
Ho	-0.055907	0.0019
Present	-0.05566	0.000009
Lindroth	-0.05566	0.00001
Present	-0.05557	0.00014
Lindroth	-0.05558	0.0001

^aRef. [19] ^bRef. [21] ^cRef. [22] ^dRef. [23]

tabulated.

In Fig. 7 the first two resonances are dominated by configurations of the form $n_1\ell_1n_2\ell_2$, where $n_1 = n_2 = 3$ and $n_1 = 3, n_2 = 4$. The remaining resonances are associated with Rydberg-type states. In Table II we compare the width and positions of the resonances in this energy region with other theoretical data. We again see that the present results are in excellent agreement with previous calculations.

Finally, we consider photo-double-detachment of H^- . We illustrate results for this process in Fig. 8 where we compare data for the percentage ratio for double-detachment to single-detachment with CCC results of Kheifets and Bray[17]. In this calculation we have included up to $n = 3$ physical states augmented by an additional 27 pseudo-states per angular momentum. We have used an R -matrix boundary of 60 a.u.. The calculation has also been repeated with a boundary radius of 70 a.u. and 80 a.u., including 32 and 33 pseudo-states per angular momentum, respectively. As these results are in accord with each other, we only present the results from the first model, for which we give both the smoothed and unsmoothed results. We see that present calculation is in excellent agreement with the work of Kheifets and Bray.

V. CONCLUSIONS

We have developed and implemented the theory for an IERM approach to photoionisation which, through the use of suitably constructed pseudo-states, allows accurate calculation of both single- and double-ionisation processes. This has been demonstrated by the excellent agreement obtained with other highly regarded theoretical methods, such as the CCC method of Kheifets and Bray [17] and the time-dependent close-coupling approach of Ludlow *et al.* [16], and with experiment, e.g. Samson *et al.* [15]. We have been able to describe the two-electron bound initial state and the final state, where either one or two electrons have been ejected, in terms of the same one-electron orbital basis. We are therefore confident that this approach can be successfully incorporated into a many-electron R -matrix approach, either time-dependent or time-independent, where $(N+2)$ -, $(N+1)$ - and N -electron systems would, similarly, be constructed from a single one-electron orbital basis. As such, it forms a key step in the development of a multipurpose R -matrix code for multiple-electron ejection, which will be capable of generating highly accurate data for time-dependent and

time independent process in the burgeoning areas of attosecond science and application of advanced X-ray lasers.

The IERM approach for electron collisions with atoms and ions has been extended, by inclusion of a model potential, to consider electron scattering from quasi-one-electron atoms and ions [25]. Similar modifications have been made to the IERM photoionisation codes, and photoionisation calculations, with double-ionisation, are currently being carried out on suitable ions of Ne and Ar, such as Ne^{6+} , Ne^{8+} , Ar^{8+} , Ar^{14+} and Ar^{16+} . We anticipate that data produced will be of interest in the field of attosecond science, as these ions are frequently used as the atomic/ionic target in such experiments. To extend this work further to consider general many-electron atoms and ions, additional theoretical and computational developments are underway which will allow two interacting electrons in the R -matrix external region. The current IERM codes and the recently developed 2-dimensional R -matrix propagator program, 2DRMP [26], can be used in this region and linked to a modified R -matrix internal region, thus facilitating accurate treatment of double-electron continua within an R -matrix framework [27].

Acknowledgments

The authors wish to thank Prof H van der Hart and Prof P G Burke for valuable discussions. AJK and MWMcI were supported by Northern Ireland DEL postgraduate studentships.

-
- [1] P. B. Corkum and F. Krausz, Nat. Phys. **3**, 281 (2007).
 - [2] N. Rohinger, D. Ryan, R. A. London, M. Purvis, F. Albert, J. Dunn, J. D. Bozek, C. Bostedt, A. Graf, R. Hill, S. Hau-Riege, and J. Rocca, Nature **481**, 488 (2012).
 - [3] P. G. Burke and K. T. Taylor, J. Phys. B: At. Mol. Phys. **8**, 2620 (1975).
 - [4] M. A. Lysaght, P. G. Burke, and H. W. van der Hart, Phys. Rev. Lett. **101**, 253001 (2008).
 - [5] L. R. Moore, M. A. Lysaght, J. S. Parker, H. W. van der Hart, and K. T. Taylor, Phys. Rev. A **84**, 061404(R) (2011).
 - [6] P.G. Burke, C. J. Noble, and M.P. Scott, Proc. Roy. Soc. A **410**, 289 (1987).
 - [7] T. T. Scholz, J. Phys. B: At. Mol. Opt. Phys. **24**, 2127 (1991).

- [8] M. P. Scott, T.T. Stitt, N. S. Scott, and P. G. Burke, J. Phys. B: At. Mol. Opt. Phys. **35**, L323 (2002).
- [9] H. Xu and R. Shakeshaft, Phys. Rev. A **83**, 012716 (2011).
- [10] C. L. Pekeris, Phys. Rev. **126**, 1470 (1963).
- [11] Y. H. Jiang, R. Püttner and G. Kaindl, J. Phys. B: At. Mol. Opt. Phys. **38**, 2157 (2005).
- [12] D. W. Lindle, T. A. Ferrett, P. A. Heimann and D. A. Shirley, Phys. Rev. A **36**, 2112 (1987).
- [13] P. G. Burke, K. A. Berrington, and C. V. Sukumar, J. Phys. B: At. Mol. Phys. **14**, 289 (1981).
- [14] K. Bartschat and I. Bray, J. Phys. B: At. Mol. Opt. Phys., **29** L577 (1996).
- [15] J. A. R. Samson, W. C. Stolte, Z.-X. He, J. N. Cutler, Y. Lu, and R. J. Bartlett, Phys. Rev. A **57**, 1906 (1998).
- [16] J. A. Ludlow, T.-G.Lee, and M. S. Pindzola, Phys. Rev. A. **81**, 023407 (2010).
- [17] A. S. Kheifets and I. Bray, Phys. Rev. A. **58**, 4501 (1998).
- [18] G. W. F. Drake, Nucl. Instrum. Methods Phys. Res. Sect. B **31** 7 (1988).
- [19] E. Lindroth, Phys. Rev. A **52**, 2737 (1995).
- [20] S. Miyake, P. C. Stancil, H. R. Sadeghpour, A. Dalgarno, B. M. McLaughlin, and R. C. Forrey, Astrophys. J. Lett. **709** L168 (2010).
- [21] H. R. Sadeghpour, C. H. Greene, and M. Cavagnero, Phys. Rev. A. **45**, 1587 (1992).
- [22] J. Tang, S. Watanabe, and M. Matsuzawa, Phys. Rev. A **46**, 2437 (1992)
- [23] Y. K. Ho, Phys. Rev. A **45**, 148 (1992).
- [24] Y. K. Ho and A. K. Bhatia, Phys. Rev. A **48**, 3720 (1993).
- [25] A. J. Kinnen, *PhD Thesis* (Queen’s University Belfast, 2005).
- [26] N. S. Scott, M. P. Scott, P. G. Burke, T. Stitt, V. Faro-Maza, C. Denis, and A. Maniopolou, Comput. Phys. Commun. **180**, 2424 (2009).
- [27] P. G. Burke, *R-matrix Theory of Atomic Collisions* (Springer-Verlag Berlin Heidelberg, 2011)